Matthias Reinhardt, Martin Kreuzer, Thomas Geue,
Reiner Dahint, Matthias Ballauff, and Roland Steitz*

Poly-acrylic Acid Brushes and Adsorbed Proteins

DOI 10.1515/zpch-2014-0540
Received May 27, 2014; accepted March 5, 2015

Abstract: Planar polyelectrolyte brushes are prepared by Langmuir–Schaefer based grafting of perdeuterated $(\text{styrene})_{49}$-b-$(\text{acrylic acid})_{222}$ block copolymer (dPS-b-PAA) to dPS pre-coated silicon supports with grafting density σ_{PAA} from 0.07 to 0.11 nm^{-2}. The structure of the solvent-swollen brushes, i. e. the volume fraction profile of polymer segments, ϕ_{PAA}, as a function of altitude z from the grafting plane into the liquid phase is extracted from neutron reflectivity measurements. We find that for all cases investigated $\phi_{\text{PAA}}(z)$ resembles a Gaussian profile. Although very condensed, the PAA brushes can be loaded with bovine serum albumin (BSA). The integral amount of adsorbed BSA scales linearly with grafting density. We compare our z-resolved volume fraction profile $\phi_{\text{BSA}}(z)$ of BSA on PAA brushes with existing literature on that system. It is found that a cross-over takes place in the adsorption scheme from ternary compressive, where proteins can approach the grafting surface only by compressing the brush, to ternary insertive, where proteins enter the brush with only local perturbation of the concentration profile, as a function of $R_{\text{P}}/H_{\text{max}}$, where R_{P} is the Stokes-Radius of the protein, and H_{max} is the experimentally determined maximum height of the brush.

Keywords: Polyelectrolyte Brush, Protein, Adsorption, Neutron Reflectivity, Solid-liquid Interface.

***Corresponding author: Roland Steitz,** Helmholtz-Zentrum Berlin, Institute of Soft Matter and Functional Materials, Hahn-Meitner-Platz 1, 14109 Berlin, Germany, e-mail: Steitz@helmholtz-berlin.de
Matthias Reinhardt, Martin Kreuzer, Matthias Ballauff: Helmholtz-Zentrum Berlin, Institute of Soft Matter and Functional Materials, Hahn-Meitner-Platz 1, 14109 Berlin, Germany
Thomas Geue: Paul Scherrer Institut, Laboratory for Neutron Scattering, 5210 Villigen, Switzerland
Reiner Dahint: Ruprecht-Karls-Universität Heidelberg, Applied Physical Chemistry, Im Neuenheimer Feld 253, 69120 Heidelberg, Germany

1 Introduction

Adsorption of proteins to surfaces is an ubiquitous phenomenon in daily life [1]. Therefore, the understanding, stimulation and control of protein adsorption is of broad academic and applied interest. Manipulation of adsorption might start by functionalizing surfaces and interfaces by grafting polymers to the underlying substrates thereby changing surface chemistry and topography [2]. In particular, solvent-swollen polymer brushes can provide a soft micro-environment for adsorbed proteins that prevents conformational and structural changes, thus maintaining protein function, or even enhances the activity of the immobilized species [1, 3–8]. Dependent on polymer chemistry these brushes can further react to external stimuli which in turn can change their protein immobilization capacity. Most prominent is the effect of the ionic strength of the dispersing medium which can alter a brush system from protein adsorbing to protein repellant [9]. A widely studied model, and quantitatively analyzed for both spherical (SPB) and planar polyelectrolyte brushes (PPB), is the adsorption of bovine serum albumin (BSA) to polyacrylic acid (PAA) brushes [10–22]. Here, the amount of immobilized BSA depends on the external parameters pH, ionic strength and protein concentration of the aqueous liquid phase and, in addition, on the internal parameters grafting density and PAA chain length. In contrast to the external parameters, which are easily controlled and manipulated in the experiments, grafting density and PAA chain length are typically fixed. A variation of grafting density and chain length is only achieved in the course of the preparation of the brushes. Most "grafting from" methods start directly from the substrate by in-situ growth of the brush system by atom transfer radical polymerization (ATRP [23, 24]). This way, however, grafting density is not well controlled. For "grafting to" methods, in particular when utilizing amphiphilic diblock-copolymers [25, 26] that weakness can be overcome. In the latter case the grafting density of the resulting polymer brush is pre-adjusted by manipulating the precursor Langmuir layer in a well-defined and reproducible manner before transferring the brush by Langmuir–Schaefer technique to solid support.

In this study we used the Langmuir–Schaefer technique to prepare PAA brushes with varied grafting density. The resulting systems were analyzed by X-ray reflectometry (XRR) in dried and neutron reflectometry (NR) in solvent-swollen state. Subsequently, BSA was adsorbed from solution to the solvent-swollen brushes at pH = 6.1, i. e. above the isoelectric point of acrylic acid. We compare our findings with existing z-resolved data on the same system, i. e. planar and spherical PAA-brushes and adsorbed BSA at comparable experimental conditions of grafting density, pH and temperature, T [13, 17, 18]. We classify the exper-

imental results within the context of recent theories on protein adsorption [27, 28] and brush structure [29].

2 Materials and methods

2.1 Materials

Disk-shaped silicon substrates (60 mm in diameter and 10 mm in height) were supplied by Siliciumbearbeitung Holm (Tann/Ndb., Germany). Perdeuterated polystyrene (dPS; $M_w = 65400$; PDI 1.02) was purchased from Polymer Standard Service (Mainz, Germany). Diblock copolymer perdeuterated $(\text{styrene})_{49}$-b-$(\text{acrylic acid})_{222}$ (dPS-b-PAA; $M_w = 21500$; PDI 1.13) was bought from Polymer Source (Montreal, Canada). D_2O (> 99.9%), Bovine serum albumin (BSA; catalog number A-6003) and all other chemicals (absolute puriss. p. a.) were from Sigma-Aldrich and used as received.

2.2 Sample preparation

The silicon wafers were cleaned for 30 min in ethanol and subsequently rinsed in ultrapure water (Milli-Q, resistance > 18.2 MΩ cm). A thin film of dPS was deposited on the substrates by spin-coating (spin-coater model 6708D, SCS, Indianapolis, Indiana, USA) using a 10 mg/ml polymer solution in toluene followed by subsequent annealing at 120 °C for 20 min in an desiccator filled with Ar. For preparation and transfer of the PAA brush 10 mg of dPS-b-PAA was dissolved in 6 ml 1,4-dioxane at 60 °C for 48 h. After addition of 4 ml toluene the polymer solution with a concentration of 1 mg/ml was spread on the surface of a 10 mM 2-(N-morpholino)ethanesulfonic acid (MES) buffer solution in a Langmuir trough (R&K, Potsdam, Germany) using a Hamilton syringe [25]. The pH value of the buffer was adjusted to 6.1 using NaOH. With movable barriers at a compression of 0.6 cm^2/s the grafting density of the dPS-b-PAA monolayer was adjusted to values of $\sigma = 0.05\ nm^{-2}$, $0.1\ nm^{-2}$, $0.2\ nm^{-2}$ for samples A1, A2 and A3, respectively (see also Figure 1). The dPS-b-PAA monolayers were transferred to dPS pre-coated Si substrates applying the Langmuir–Schaefer technique by dipping the substrates onto the water surface of the Langmuir trough. The surface pressure at the transfer was monitored by the Wilhelmy plate pressure gauge of the Langmuir trough. Analysis of the surface loss area on the water surface at equal surface pressure lead to a transfer ratio of 1.3 ± 0.1. After transfer, the brushes on solid support were

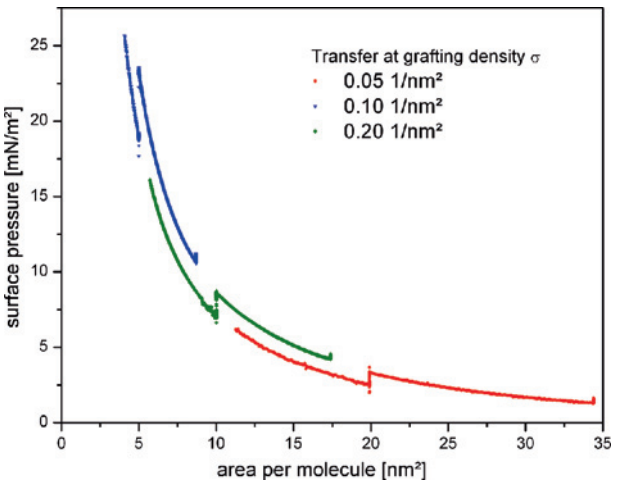

Figure 1: Surface pressure – area isotherm of free floating dPS-b-PAA monolayers at 20 °C and subphase pH 6.1. Positions of Langmuir–Schaefer transfers of the monolayers to dPS-pre-coated silicon wafers at the three different grafting densities are indicated by respective drops of surface pressure in the isotherm at 20 nm^2/molecule (red), 10 nm^2/molecule (green) and 5 nm^2/molecule (blue).

exposed to annealing at 120 °C for 15 min followed by rinsing with ultrapure water.

2.3 X-ray reflectivity

The X-ray reflectometer used was a home build 2-circle instrument with horizontal scattering geometry and a resolution $\Delta Q = 0.03\ nm^{-1}$ at a wavelength of 0.1541 nm generated by a Cu anode. Additional information on the instrument can be found elsewhere [30]. The X-ray raw data were footprint corrected and normalized to the intensity of the direct beam [31].

2.4 Neutron reflectivity

Neutron reflectivity (NR) measurements were performed at the time of flight reflectometer AMOR at SINQ, Paul Scherrer Institut (PSI), Villigen, Switzerland [32]. A full reflectivity run consisted of measurements at incident angles $\theta_1 = 0.4^\circ$, $\theta_2 = 0.8^\circ$ and $\theta_3 = 1.6^\circ$ of the white beam on the samples planar solid-liquid interface through the silicon backing. Those measurements covered a Q-range of 0.08

Table 1: Scattering length densities of materials and compounds used.

Material	X-ray SLD, SLD^x [10^{-4} nm^{-2}]	neutron SLD, SLD^n [10^{-4} nm^{-2}]
Si	20.1	2.07
SiO_2	18.9	3.46
dPS	9.51	6.42
PAA	9.44	2.34
D_2O		6.36

to 1.74 nm^{-1} in total consuming 7 h of beam-time with a resolution of $\Delta Q/Q = 7\%$ as defined by chopper system and slits. The sample cell was a high pressure cell for neutron reflectometry for pressures up to 1000 bar, with which also measurements at elevated hydrostatic pressure can be performed. Detailed information on the sample cell can be found elsewhere [33]. All measurements were conducted against 10 mM MES buffer solution in D_2O adjusted to pH = 6.1 using NaOD. For adsorption of BSA to the PAA brushes, the samples (silicon/dPS/dPS-b-PAA) were incubated outside the sample cell with 0.5 mg/ml BSA in D_2O MES buffer solution for 30 min. Before remounting, the samples were rinsed with pure buffer solution. All neutron reflectivity investigations were conducted at 20 °C with the sample cell thermostatted by an external water bath. The raw data were normalized to the measured incident intensity spectra I_0^{Si} through the silicon substrate mounted in the high pressure sample cell.

2.5 Data analysis

All reflectivity data were analyzed utilizing the Motofit software package [34], where, by the Abeles transfer matrix formalism [35], the reflectivity $R_{\mathrm{fit}}(Q)$ of model scattering length density profiles $\mathrm{SLD}(z) = \sum_i \mathrm{SLD}_i(z_i)$ of stratified media [36] were calculated and compared with the experimental data, $R(Q)$.

In case of the XRR measurements on the brushes in dried state we subdivided the system in three parts – collapsed PAA brush layer, dPS (anchor and precoating) layer and silicon support from top to bottom. The native SiO_2 layer, sandwiched between dPS layer and silicon support, was included in the roughness of the dPS-silicon interface. We found this a reasonable procedure as the scattering length densities of SiO_2 and Si for X-rays are very close (see Table 1). Attempts to fit that layer resulted in thickness smaller than roughness. The collapsed PAA brush against air was modeled by a series of i slabs of fixed thickness $d_i = 0.7$ nm and varied scattering length density SLD_i. A thickness of 0.7 nm corresponds to a Q_z

value of 9 nm^{-1}, which is 1.5 times larger than the maximum momentum transfer, $Q_{max} = 6\ nm^{-1}$, probed in the conducted XRR measurements. Hence, artificial interferences in the calculated reflectivity curves used for fitting are avoided. The required number i of slices representing the collapsed PAA brush layer were an outcome of the fitting process.

For the neutron measurements at the solid-liquid interface we subdivided the system into silicon backing, dPS (pre-coating + anchor) layer of the brush, PAA brush layer and buffered D_2O fronting phase from top to bottom with respect to the incident beam. The native SiO_2 layer, sandwiched between silicon support and the dPS pre-coating, was included in the roughness of the silicon-dPS interface. The dPS layer was represented by one box of thickness d_{dPS} as extracted from the preceeding X-ray measurements. The solvent-swollen PAA brush was divided into slices of 2 nm thickness each with no inter-layer roughness. The reciprocal width of the chosen strata was twice the maximum momentum transfer Q_{max} probed experimentally. The required number i of slices representing the PAA brush were outcome of the fitting process.

The neutron scattering length density of PAA was calculated to $SLD^n_{PAA} = 2.34 \times 10^{-4}\ nm^{-2}$ at an acrylic acid monomer mass density of 1.051 g/cm^3 [37] and the hydrogen of the acid group presumed exchanged by deuterium in contact with the D_2O fronting phase [37, 38]. Starting at the grafting plane $z = 0$ defining the dPS/PAA interface position the scattering length density $SLD(z)$ of any given slice of 2 nm thickness of the solvent-swollen PAA brush in D_2O is given by the binary mixture of PAA and D_2O in that slice. Hence,

$$SLD(z) = \phi_{PAA}(z)SLD^n_{PAA} + (1 - \phi_{PAA}(z))SLD^n_{D_2O} \tag{1}$$

where

$$\phi_{PAA}(z) = \frac{SLD(z) - SLD^n_{D_2O}}{SLD^n_{PAA} - SLD^n_{D_2O}} \tag{2}$$

is the volume fraction profile of the PAA brush. The SLDs of all materials used in this work are summarized in Table 1.

The statistical errors for a single fit within Motofit for all measurements conducted were smaller than 5% in thickness and 5% in scattering length density.

Table 2: Grafting densities σ_{XRR} from X-ray reflectometry measurements on samples A1–A3.

Sample	σ_{XRR} [nm^{-2}]			
	prepared	transferred	annealed	rinsed
A1	0.05	0.07 ± 0.01	0.13 ± 0.01	not measured
A2	0.10	0.13 ± 0.01	0.22 ± 0.02	0.08 ± 0.01
A3	0.20	0.26 ± 0.02	not measured	0.11 ± 0.01

3 Results

3.1 Brushes at the solid-air interface

We controlled the preparation of the PAA brushes by X-ray reflectometry. Figure 2 depicts the respective measurements on sample A2 conducted before and after transfer of the dPS-b-PAA Langmuir layer with the sample in a dried state. From the scattering length density profiles in Figure 2b, the grafting density σ_{XRR} was extracted as

$$\sigma_{XRR} = \frac{1}{Zr_e} \int_{0\,\mathrm{nm}}^{8\,\mathrm{nm}} \left(\mathrm{SLD}''(z) - \mathrm{SLD}'(z) \right) dz \tag{3}$$

where $\mathrm{SLD}'(z)$ and $\mathrm{SLD}''(z)$ are the fitted SLD profiles prior to and after LS transfer (and after rinsing), $Z = 11572$ is the total number of electrons of one dPS-B-PAA molecule and $r_e = 2.82 \times 10^{-15}$ m is the Thompson radius of the free electron. The extracted grafting densities are summarized in Table 2. The values measured after the transfer of the brushes and the annealing step were found to be a factor of 2 larger than expected. Most likely with the transfer of the PAA brushes also excess water and additional polymer was transferred. The water evaporated in the course of the subsequent annealing step and left excess polymer behind. Only by extensive subsequent rinsing with ultra-pure water that material, i. e. buffer salt and any non-grafted polymer, was removed. The final grafting densities are gathered in the last column of Table 2.

3.2 Brushes at the solid-liquid interface

Figure 3a shows NR data and fits for the re-swollen PAA brushes (A1–A3) against buffered D_2O subphase at ambient conditions. All spectra exhibit characteristic Kiessig oscillations. The width of these oscillations depends on the thickness of

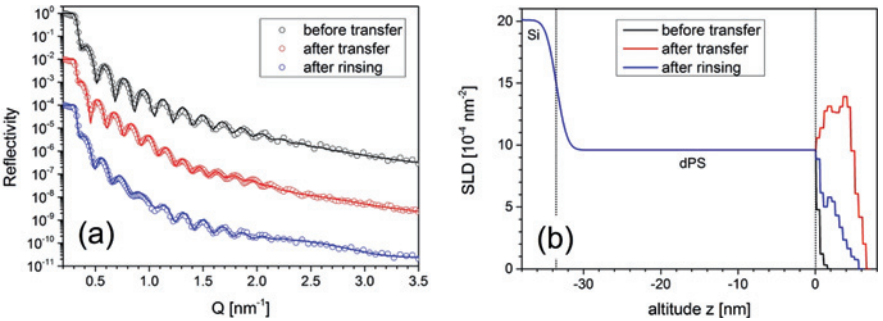

Figure 2: X-ray reflectivity (a) and extracted SLD profiles (b) of sample A2, transferred at a pre-adjusted lateral density on the water surface of $\sigma = 0.1\ \mathrm{nm}^{-2}$. Measurements were taken before transfer, i. e. on the dPS-precoating on silicon support (black), after transfer (red) and after rinsing (blue). Solid lines are fits to the data.

Table 3: Gaussian parameters of solvent-swollen brushes at the solid-liquid interface.

Sample	σ_{NR} [nm^{-2}]	ϕ_0	H_0 [nm]
A1	0.071 ± 0.007	0.62 ± 0.06	3.26 ± 0.07
A2	0.083 ± 0.008	0.56 ± 0.06	4.13 ± 0.14
A3	0.108 ± 0.010	0.60 ± 0.06	4.89 ± 0.24

the dPS sublayer while shape and height are related to the conformation of the protonated PAA brush. Figure 3b shows the extracted SLD profiles for the PAA brushes and Figure 3c gathers the resulting polymer brush volume fraction profiles based on (2). These profiles exhibit a Gaussian shape described by the function:

$$\phi_{\mathrm{Gauss}}(z) = \phi_0 e^{-\frac{z^2}{H_0^2}} \tag{4}$$

with volume fraction ϕ_0 at the grafting plane $z = 0$ and thickness H_0. The grafting density is independently determined from the NR measurements by integration over the volume fraction profile $\phi_{\mathrm{PAA}}(z)$:

$$\sigma_{\mathrm{NR}} = \frac{1}{N v_{\mathrm{PAA}}} \int_{0\ \mathrm{nm}}^{18\ \mathrm{nm}} \phi_{\mathrm{PAA}}(z) dz \tag{5}$$

$v_{\mathrm{PAA}} = 0.1137\ \mathrm{nm}^3$ is the acrylic acid monomer volume and $N = 222$ is the degree of polymerization. The extracted brush parameters are compiled in Table 3. Interestingly, $\phi_0 \approx 0.60 \pm 0.05$ and is independent of the grafting density σ. Therefore, H_0 scales with σ.

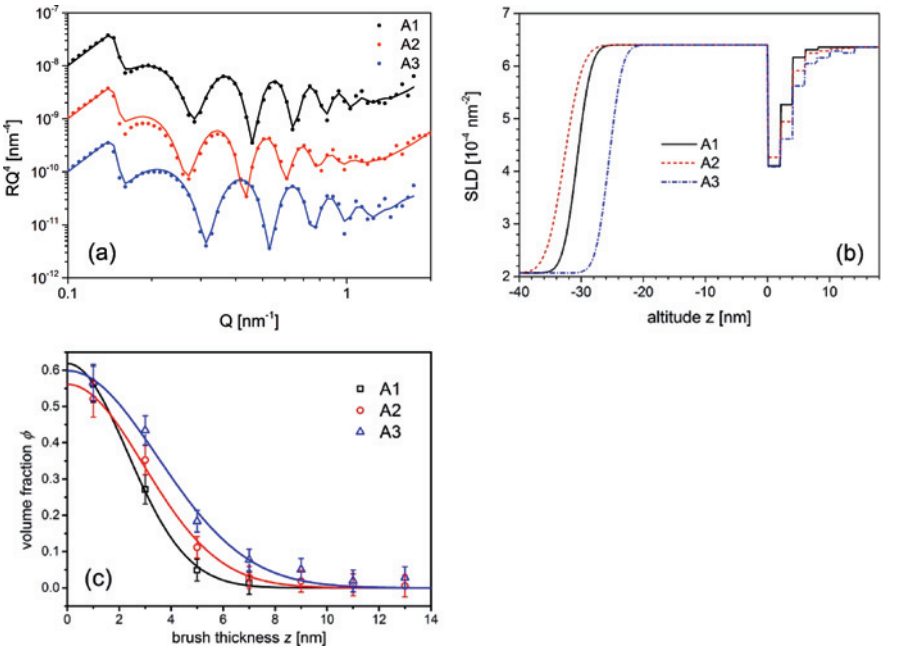

Figure 3: Neutron reflectivity (a), extracted SLD profiles (b) and volume fraction profiles (c). Data sets in (a) are offset by factors of 10 on the y-axis for clarity. Solid lines in (a) and (c) are fits to the data.

3.3 Protein adsorption

Figure 4a shows the change of the NR data and fits after the adsorption of BSA to the PAA brushes. The shift of the Kiessig oscillations towards lower Q refers to an increase in brush thickness. This is a direct indication of a successful binding of BSA proteins to the PAA brushes. The extracted SLD profiles are displayed in Figure 4b. When BSA adsorbs to the PAA brush, D_2O is replaced by the protein [13, 18]. The neutron SLD of BSA, $SLD_{BSA} = 3.19 \times 10^{-4}$ nm^{-2} [39], is lower than that of D_2O, resulting in a decreased SLD of the respective slab in the box model (cf. Figure 4b). Integration over the difference of the SLD profiles before and after adsorption of BSA yields the adsorbed mass of BSA per surface area, Γ_{BSA}

$$\Gamma_{BSA} = \frac{M_{BSA}}{V_{BSA}} \int_z \frac{SLD^*(z) - SLD(z)}{SLD^n_{BSA} - SLD^n_{D_2O}} dz \tag{6}$$

where $SLD(z)$ and $SLD^*(z)$ are the extracted SLD profiles before and after protein adsorption, $M = 66\,267$ g/mol is the molar mass and $V = 48\,574$ cm^3/mol (80.660 nm^3/molecule) is the molar volume of BSA [39]. The calculated amount

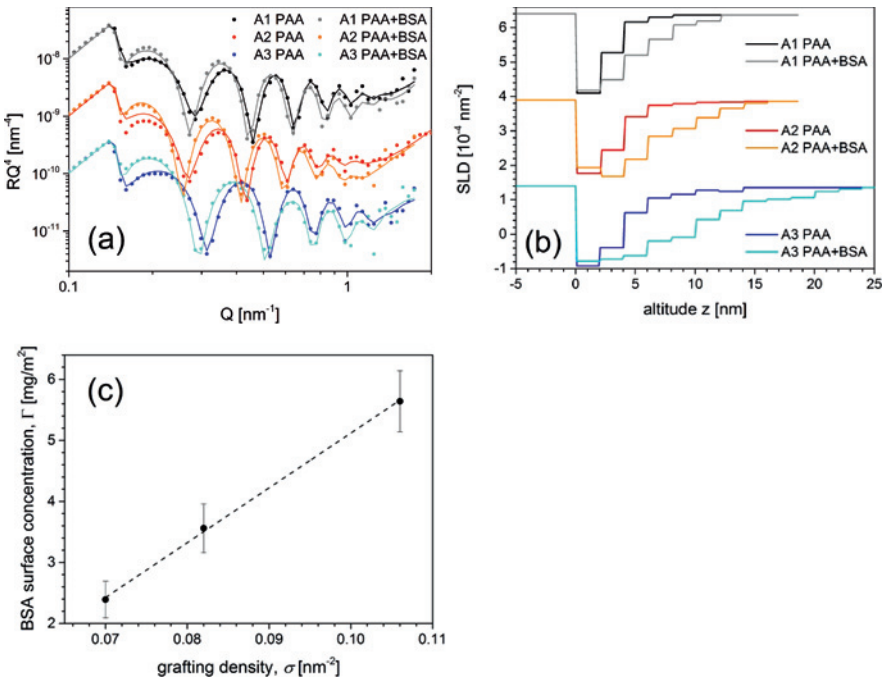

Figure 4: (a): Neutron reflectivity data and fits for the PAA brushes A1–A3 before and after adsorption of BSA. For visualization, respective data sets are offset by factors of 10 on the y-axis. (b): extracted SLD profiles of the PAA brushes A1–A3 before and after adsorption of BSA. For visualization, SLD data of A2 are offset by factors of $-2.5 \times 10^{-4}\ \mathrm{nm}^{-2}$ and SLD data of A3 are offset by factors of $-5 \times 10^{-4}\ \mathrm{nm}^{-2}$ on the y-axis. (c): Adsorbed amount of BSA over grafting density of samples A1–A3. Γ_{BSA} scales linear with σ.

of adsorbed protein per surface area for the three measured grafting densities is shown in Figure 4c. A linear correlation between adsorbed amount of protein and grafting density is found.

4 Discussion

4.1 Brush structure

The preparation of brushes from dPS-b-PAA block-copolymer with varied grafting density worked well. In their solvent-swollen state at the solid-liquid interface all brushes exhibit a Gaussian shape with a maximum volume fraction $\phi_0 \approx 0.60$ at

the grafting plane. The Gaussian conformation is in qualitative agreement with theoretical self-consistent field (SCF) calculations [29, 40, 41] and experimental results [42, 43]. PAA brushes belong to the class of weak annealed polyelectrolyte brushes for which Zhulina and Borisov derived a diagram of states [29]. For direct comparison, we transferred the physical parameters of our PAA brushes and the experimental boundary conditions into their reduced counterparts t, ν, u and Φ as given in Equations (38)–(41) of reference [29].

$$\text{Reduced distance: } t = bz = \sqrt{\frac{3\pi^2}{8}}\frac{z}{aN} \tag{7}$$

$$\text{Reduced polymer coverage: } \nu = 4\sqrt{\frac{2}{3}}\frac{al_{\mathrm{B}}N^2}{s} \tag{8}$$

$$\text{“Strength” of tethered polyacid: } u = \frac{16}{3\pi}a^2 l_{\mathrm{B}} K_{\mathrm{a}} N^2 \tag{9}$$

$$\text{Relative salt content: } \Phi = \frac{c_{\mathrm{s}}}{c_{\mathrm{H}}^{+}} \tag{10}$$

with a, the length of an AA monomer in nm, l_{B}, the Bjerrum length of water in nm, s, the grafting area per AA chain in nm^2, K_{a}, the dissociation constant of an AA monomer, c_{S}, the salt concentration in mol/l and c_{H}^{+}, the concentration of hydrogen ions in mol/l.

The monomer density profile $c_{\mathrm{AA}}(z)$ of the acrylic acid (AA) brush segments is given by $c_{\mathrm{AA}}(z) = \phi(z)$ with the monomer volume V_{AA} of 0.1137 nm^3 at a mass density of 1.051 $\mathrm{g/cm}^3$. A single PAA polymer chain consists of $N = 222$ monomer units with monomer length $a \approx \sqrt[3]{6V_{\mathrm{AA}}\pi} \approx 0.60$ nm. The chains are grafted to the interface at a grafting density $\sigma = 1/s$, where s is the grafting area per chain. For $\sigma \approx 0.1\ \mathrm{nm}^{-2}$, $s \approx 10\ \mathrm{nm}^2$. The ionic strength of the 10 mM monovalent buffer is $I = c_{\mathrm{S}} = 10$ mM. The concentration of hydrogen, c_{H}^{+}, here the concentration of deuterium ions, $c_{\mathrm{D}}^{+} = 8 \times 10^{-7}$ mol/l, is set by the pH = 6.1 of the D_2O buffer solution. The dissociation constant K_{a} of an AA monomer unit is given by its pK_{a}, which is 4.35 for free acrylic acid monomers [44]. For polymerized acrylic acid the pK_{a} shifts to higher values depending on salt concentration and degree of polymerization [45]. For the PAA brushes used in this work, the pK_{a} approximately equals the pH value of the buffer solution and thus $K_{\mathrm{a}} = 8 \times 10^{-7}$ mol/l. The degree of ionization, α_b, as determined by the mass action law $\alpha_b/(1-\alpha_b)K_{\mathrm{a}}c_{\mathrm{D}}^{+}$ equals 0.5. The Bjerrum length l_{B} of water at 25 °C is 0.71 nm.

With the experimentally specified set, $b \approx 0.014\ \mathrm{nm}^{-1}$, $\nu \approx 6857$, $u \approx 0.017$ and $\Phi = 7581$, our PAA brushes are located in the osmotic annealing regime of the Zhulina-Borisov diagram of states (cf. Figure 2 in ref [29]). In this regime both polymer density and electrostatic potential vary substantially throughout the brush. The degree of ionization $\alpha(z)$ also varies and the value $\alpha(0)$ at the grafting plane

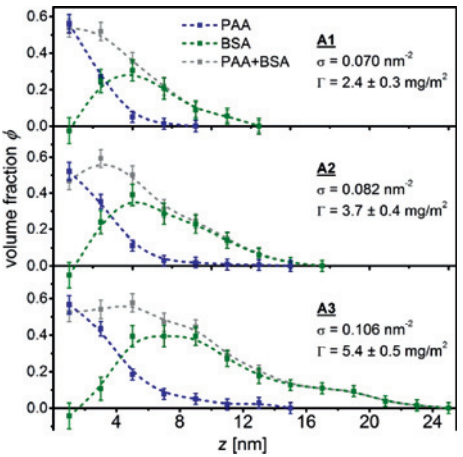

Figure 5: Volume fraction profiles of the conserved PAA brush and adsorbed BSA for samples A1–A3. Smoothed lines are added to guide the eye.

differs significantly from the value $\alpha(H_0) \approx \alpha_b$ for the chain ends stretched into the buffer solution. The theoretically calculated density profile for a PE brush in the osmotic annealing regime exhibits a characteristic Gaussian shape, which qualitatively compares well with our experimental results.

4.2 Protein adsorption

4.2.1 Spatial distribution of BSA inside planar PAA brushes

Information on the integral amount of adsorbed proteins to polymer brushes is also available using lab-based methods such as ultra-filtration in case of spherical polyelectrolyte brushes [12] or optical reflectometry [20] and surface plasmon resonance spectroscopy [21] in case of planar brushes. The advantage in utilizing NR is in the extraction of information on the spatial distribution of bound proteins inside the polymer brushes. In this work, with only one scattering contrast available, it was not possible to directly distinguish the z-resolved mixing ratio of BSA, PAA and D_2O. The profile for one of the components had to be fixed by an initial presumption. A first intuitive assumption is that there is no conformational change of the PAA brush upon loading with BSA in concordance with literature [13]. In this case of a conserved PAA brush the z-resolved BSA volume fraction profile $\phi_{BSA}(z)$ can be extracted directly from the difference of the SLD

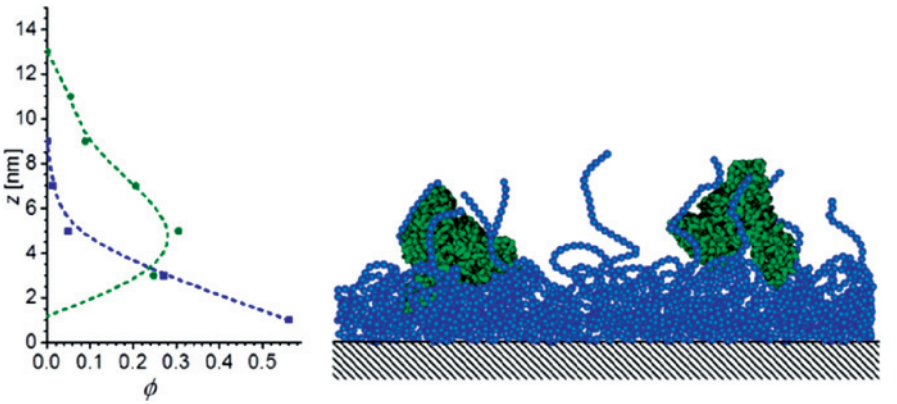

Figure 6: Schematic PAA and BSA volume fraction profiles for the conserved PAA brush model based on the analysis of sample A1 (cf. also Figure 3, bottom panel and Figure 5).

profiles [13]:

$$\phi_{\mathrm{BSA}}(z) = \frac{\mathrm{SLD}^{*}(z) - \mathrm{SLD}(z)}{\mathrm{SLD}^{n}_{\mathrm{BSA}} - \mathrm{SLD}^{n}_{\mathrm{D_2O}}} \tag{11}$$

The extracted volume fraction profiles are shown in Figure 5.

Within the error of the calculated profiles, the presumption of a conserved PAA brush results in a small negative adsorbed amount of protein close to the grafting plane of the brush. This result may indicate a potential stretching of the PAA brush with the adsorption. An assumed stretching of the PAA brush profile also changes the BSA volume fraction profile. This leads to a second model of a stretched PAA brush. At first, we will discuss the results for the conserved PAA brush (model I) followed by a debate of the results for the stretched PAA brush (model II).

4.2.2 Conserved PAA brush

The PAA brush adopts a very dense structure with PAA volume fractions $\phi > 0.50$ in the first 2 nm slab near the grafting plane to the dPS sublayer. Dense polymer brushes are known to be resistant to protein adsorption [46]. Compared with our small brush, BSA is a relatively big molecule with lateral dimensions in the range of 6–8 nm [39, 47, 48], with a mean (Stokes) radius $R_{\mathrm{P}} \approx H_0$.

Proteins that are large compared to the brush ($R_{\mathrm{P}} \geq H_o$) can approach the surface only by compression of the polymer brush [28, 46, 49]. The free energy penalty, associated with compression and compaction of the brush, favors sec-

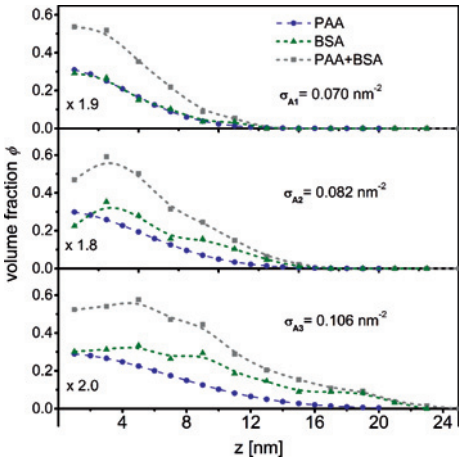

Figure 7: Volume fraction profiles of stretched PAA brushes and adsorbed BSA. Smoothed lines are added to guide the eye.

ondary adsorption of the protein at the outer surface of the brush [46]. The extracted protein volume fraction profiles of Figure 5 directly support this model. Especially for the lowest and the intermediate grafting densities, $\sigma = 0.07$ and $0.082\ \mathrm{nm}^{-2}$, (sample A1 and A2) the volume fraction profile of adsorbed BSA describes the adsorption of a BSA monolayer on top of the dense part of the PAA brush (Figure 6). The volume fraction profile of BSA at highest brush grafting density is more spread out in altitude z and indicates adsorption of a second layer. In all cases investigated there is a pronounced separation of the centers of gravity, c_m, of brush and adsorbed protein, ranging from an offset $\Delta_z^{c_m}$ from 3.9 (A1) to 6.7 nm (A3). The dangling PAA chain ends provide a soft environment for the adsorbed proteins, while the dense PAA inner layer screens the hydrophobic dPS sublayer and thus helps to preserve the native protein structure [10, 11].

4.2.3 Stretched PAA brush

If the brush is stretched upon adsorption of BSA, an assumption has to be made to describe the resultant PAA brush profile. Our simple model II proposes a linear stretching of the PAA brush by a factor based on the difference of its rms-thickness [50] before and after protein adsorption. Based on Figure 5, middle panel, a mean stretching factor of 1.9 ± 0.2 was extracted this way, resulting in brushes that were extended to nearly twice their original length upon adsorption of BSA. Modifications were applied to the Gaussian PAA brush profiles with the

Table 4: Number κ of bound BSA molecules per PAA chain in relation to the grafting density σ.

Sample	σ_{NR} [nm^{-2}]	Γ [mg/m^2]	κ [BSA/PAAchain]
A1	0.070 ± 0.007	2.4 ± 0.3	0.31 ± 0.06
A2	0.082 ± 0.008	3.6 ± 0.4	0.40 ± 0.08
A3	0.106 ± 0.010	5.6 ± 0.5	0.48 ± 0.09

respective stretching factors calculated individually for samples A1–A3. Figure 7 shows the resulting volume fraction profiles. The profiles of adsorbed BSA follow the profiles of the PAA brush. A non-zero volume fraction of BSA is found directly at the grafting interface to the dPS sublayer, supporting primary adsorption.

4.2.4 Comparison of conserved and stretched PAA brush models after protein adsorption

Figures 5 and 7 show the volume fraction profiles of PAA and BSA after adsorption on the presumptions of conserved and stretched PAA brushes, respectively. The main difference between the models is the adsorption of BSA either on top of the dense PAA screening layer in case of the conserved PAA brush or the penetration of BSA into this layer down to the dPS grafting plane in case of the stretched PAA brush. Purely based on the available experimental data both models seem qualified in describing the adsorption of BSA. In case of the conserved brush, the non-physical negative amount of adsorbed BSA can be set to zero within error. The adsorption on top of the dense PAA screening layer is consistent with the protein resistance of dense polymer structures [46]. Also the preservation of the protein structure, as indicated by the volume fraction profile of BSA, supports zero adsorption next to the hydrophobic dPS sublayer, in-line with literature [10, 11].

The adsorption on top of the planar PAA brush seems to be in contradiction to measurements on spherical polyelectrolyte brushes (SPB). There, BSA was found deep inside the PAA brush [16, 17]. These results favor the extracted BSA density profiles based on the stretched PAA brush model. However, direct comparison of SPB brushes and the planar brushes in this work is not straightforward. The thickness of the spherical PAA brushes was larger than 50 nm and thus 3–5 times bigger than the maximum thickness of the planar PAA brushes used here. In a brush with a thickness of $t > 50$ nm a dense 2–3 nm thick screening (carpet) layer at the grafting plane is negligible. The diluted part of the spherical PAA brush accessible to protein adsorption amounts to 95%. For the smaller planar brushes in this work the dense screening or carpet layer covers up to 30% of the total brush

thickness and thus directly affects the protein adsorption. Hence, the adsorption of BSA on top of dense, thin PAA brushes, as suggested by the model of the conserved brush, is not in contradiction to existing results on the adsorption of BSA inside thick spherical PAA brushes. Taken the protein resistance of dense polymer brushes into account, the conserved PAA brush model seems preferable over the model of the stretched brush.

Up to this point our comparison between the conserved and stretched brush model was exclusively based on the protein distribution with respect to the PAA brush profile, irrespective of the integral amount of bound BSA. With increasing grafting density σ the integral amount Γ of adsorbed BSA also increases in a linear fashion (Figure 5, bottom). The latter is not true for the ratio $\kappa = \Gamma/(\sigma \cdot m_{\mathrm{BSA}})$ of the average number of bound BSA per PAA chain, where $m_{\mathrm{BSA}} = 1.1 \times 10^{-19}$ g is the mass of a single BSA molecule [39]. With increasing grafting density σ, κ increases in a non-linear fashion (see Table 4).

If BSA can bind to any position inside the PAA brush, as is the case for the stretched PAA brush, κ is expected to be constant. In case of the conserved PAA brush, the dense PAA screening layer is not penetrated by BSA. Adsorbed proteins are found exclusively in the diluted outer part of the brush. With the completion of the screening layer, its relative contribution to the total brush thickness should decrease with increasing grafting density, i. e. further stretching. Thus, κ should converge to a plateau value in the long chain limit, where the contribution of the screening layer to the total brush length was negligible. Our experimental results gathered in Table 4 are in line with such expectation. Hence, also the extracted integral amount of adsorbed BSA proteins supports the model of the conserved PAA brush.

4.3 Comparison with literature

4.3.1 Relevant length scales

Following a very basic scheme, we can subdivide protein adsorption to polymer brushes into primary, secondary and ternary adsorption [27]. In case of primary adsorption the radius R_{p} of the immobilized protein is smaller than the mean distance between graft points of the polymer chains, i. e. $R_{\mathrm{p}} < 1/\sqrt{\sigma}$, and the protein adsorbs at the grafting plane. In case of secondary adsorption, R_{p} is much larger than the mean distance between graft points, i. e. $R_{\mathrm{p}} \gg 1/\sqrt{\sigma}$, and consequently, the protein is not to penetrate the brush and adsorbs at the outer surface. In case of matching quantities, $R_{\mathrm{p}} \approx 1/\sqrt{\sigma}$, we are in the ternary regime and the protein molecules adsorb to polymer segments within the brush. Halperin and

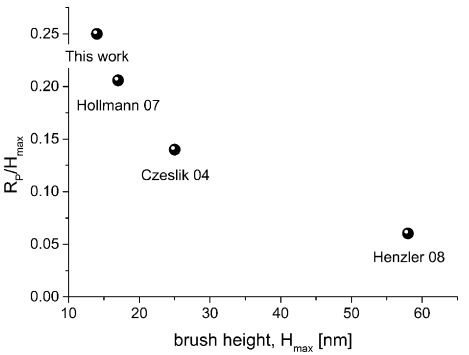

Figure 8: Stokes Radius R_P of BSA normalized on brush height $H_{\max}$ and plotted versus $H_{\max}$. Here, $H_{\max}$ is the maximum height of the brush as read out from the experimental SLD profiles shown in the respective papers.

Kröger further differentiate the latter regime into strong and weak ternary adsorption [28]. Due to the lack of specific binding sites, our system, PAA + BSA, is placed within the weak ternary adsorption regime. According to Halperin and Kröger that regime comes in two modes, namely ternary insertive, where small proteins with $R_{\mathrm{P}} \ll H_0$ enter the brush with only local perturbation of the concentration profile, and ternary compressive, where large proteins with $R_{\mathrm{P}} \gg H_0$ can approach the grafting surface only by compressing the brush of height H_0 (cf. Figure 2 in ref [28]).

In Figure 8 we list available data on the system PAA + BSA in accordance with the Halperin and Kröger criteria laid out above.

In this plot the condition of secondary adsorption is realized for $R_{\mathrm{P}}/H_{\max} \geq 0.5$, while ternary adsorption in insertive mode to primary adsorption is given for $H_{\max} \to \infty$ and thus $R_{\mathrm{P}}/H_{\max} \to 0$. Our system is located halfway between the endpoints. Consequently and as shown already in paragraph 4.2.1 from the z-resolved volume fraction profiles we are dealing here with the ternary adsorption of BSA to short PAA brushes in compressive mode. As the length $H_{\max}$ of brushes increases the adsorption mode of BSA changes continuously until an experimental endpoint is reached at $R_{\mathrm{P}}/H_{\max} = 0.05$ for the spherical brushes in the work by Henzler et al. [17].

4.3.2 Scaling

Except for the spherical PAA brushes utilized by Henzler et al. [17], all brush systems compared here are prepared by the grafting-to technique via Langmuir pre-

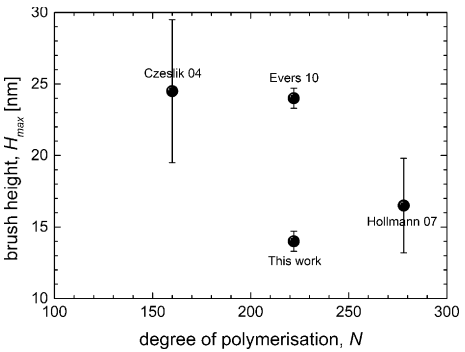

Figure 9: Experimentally determined brush height $H_{\max}$ versus degree of polymerization N of the utilized PAA polymers.

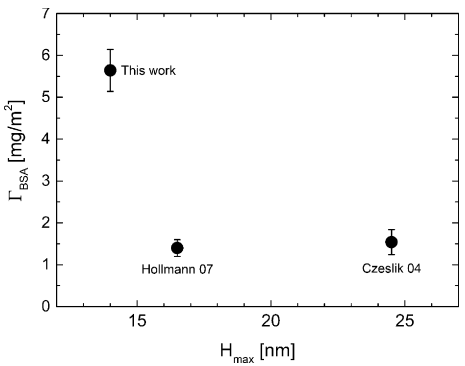

Figure 10: Adsorbed amount of BSA on planar PAA-brushes at $\sigma = 0.1\ \mathrm{nm}^{-2}$ as a function of height $H_{\max}$of the brushes at the solid-liquid interface.

cursors of PS-b-PAA block-copolymers. The latter brushes all come with an experimentally adjusted grafting density of $0.1\ \mathrm{nm}^{-2}$ and are exposed to an aqueous phase of pH 6–7 at room temperature. For the very reason one would expect the brush height $H_{\max}$ of the investigated systems to scale with the degree of polymerisaton N of the PAA blocks, i. e. $H_{\max} \propto N$. From Figure 9 it becomes obvious that this simple scaling prediction is violated experimentally. On the best the height of the prepared brushes is independent of N with a statistical average height $\bar{H}_{\max}$ of 20 ± 5 nm for a statistical span of $\bar{N}$ of 220 ± 48. The most positive conclusion one can draw here is that the variation in N is simply too little to be effective, the most negative one is to state that there is at minimum one additional experimental parameter influencing the final brush height which is out of control. Such parameter could be an intermediate annealing step or intermediate drying

of the brushes. A broader data base, in particular with a much larger variation of N, is required to clarify this issue.

4.3.3 Adsorbed amount

The total adsorbed amount of BSA scales linearly with the grafting density of the PAA brush (Figure 5, bottom) in line with an increasing number of binding sites per unit area and in line with results by optical reflectometry [20]. Figure 10 depicts the adsorbed amount of BSA on planar PAA brushes which can be compared directly. Interestingly the shortest brush seems to immobilize the largest amount of protein. The picture changes immediately when taking into account the fact that the adsorbed amount of protein also depends on the protein concentration of the aqueous reservoir [51, 52]. Hollmann [18] and Czeslik [13] used bulk concentrations, c_{eq}, of BSA, which were 1/10 of the one we used on this work, namely 0.05 mg BSA/ml (Hollmann 07, Czeslik 04) as compared to 0.5 mg BSA/ml (this work). Hence, comparison of published data is not straight forward without correcting for c_{eq}, incubation time, incubation temperature and potentially further boundary conditions which have to be taken into consideration.

5 Summary and conclusions

Solvent-swollen planar PAA brushes at three different grafting densities were investigated by neutron reflectivity at the solid-liquid interface before and after incubation with BSA at ambient conditions. The extracted Gaussian volume fraction profiles of the brushes are in line with theoretical predictions for osmotically annealed brushes. Differences are found for the detailed stretching of the brushes. These might be caused by additional interactions at the grafting plane. The experimentally observed increased density of PAA near the anchoring plane might originate from screening of the hydrophobic dPS sublayer from the D_2O subphase. BSA adsorbs to the PAA brushes from solution. The adsorbed amount of protein scales linear with the grafting density of brushes. As for the distribution of BSA within the PAA brushes, two different structural models are considered: Model I presumes conservation of PAA brush structure upon BSA adsorption, model II favors affine stretching of the brushes by a factor of 2. In model I the BSA molecules would not penetrate but were adsorbed at the surface of the brushes following a secondary adsorption scenario. On the contrary, in model II, BSA molecules would penetrate resulting in a homogenous distribution of protein

inside the brushes as was expected for weak ternary adsorption. From comparison with literature both on experimental systems and theory of protein adsorption to brushes we classify our case as weak ternary adsorption in compressive mode.

Acknowledgement: This work is based on experiments performed at the Swiss spallation neutron source SINQ, Paul Scherrer Institut (PSI), Villigen, Switzerland. The authors thank Helmholtz-Zentrum Berlin and Paul Scherrer Institut for financial support.

References

1. C. Czeslik, Chem. Unserer Zeit **40** (2006) 238.
2. V. Papaefthimiou, R. Steitz, and G. H. Findenegg, Chem. Unserer Zeit **42** (2008) 102.
3. C. Jeworrek, O. Hollmann, R. Steitz, R. Winter, and C. Czeslik, Biophys. J. **96** (2009) 1115.
4. N. Ayres, Polymer Chem. **1** (2010) 769.
5. A. Wittemann and M. Ballauff, Phys. Chem. Chem. Phys. **8** (2006) 5269.
6. A. L. Becker, K. Henzler, N. Welsch, M. Ballauff, and O. Borisov, Curr. Opin. Colloid In. **17** (2012) 90.
7. K. Henzler, B. Haupt, K. Lauterbach, A. Wittemann, O. Borisov, and M. Ballauff, J. Am Chem. Soc. **132** (2010) 3159.
8. N. Welsch, A. Wittemann, and M. Ballauff, J. Phys. Chem. B **113** (2009) 16039.
9. C. Czeslik, G. Jackler, T. Hazlett, E. Gratton, R. Steitz, A. Wittemann, and M. Ballauff, Phys. Chem. Chem. Phys. **6** (2004) 5557.
10. C. Reichhart and C. Czeslik, Langmuir **25** (2009) 1047.
11. A. Wittemann and M. Ballauff, Anal. Chem. **76** (2004) 2813.
12. A. Wittemann, B. Haupt, and M. Ballauff, Phys. Chem. Chem. Phys. **5** (2003) 1671.
13. C. Czeslik, G. Jackler, R. Steitz, and H. H. von Grunberg, J. Phys. Chem. B **108** (2004) 13395.
14. A. Wittemann, B. Haupt, and M. Ballauff, Z. Phys. Chem. **221** (2007) 113.
15. O. Hollmann and C. Czeslik, Langmuir **22** (2006) 3300.
16. S. Rosenfeldt, A. Wittemann, M. Ballauff, E. Breininger, J. Bolze, and N. Dingenouts, Phys. Rev. E (2004) 70.
17. K. Henzler, S. Rosenfeldt, A. Wittemann, L. Harnau, S. Finet, T. Narayanan, and M. Ballauff, Phys. Rev. Lett. **100** (2008) 158301.
18. O. Hollmann, T. Gutberlet, and C. Czeslik, Langmuir **23** (2007) 1347.
19. J.H. Dai, Z. Y. Bao, L. Sun, S. U. Hong, G. L. Baker, and M. L. Bruening, Langmuir **22** (2006) 4274.
20. W. M. de Vos, P. M. Biesheuvel, A. de Keizer, J. M. Kleijn, and M. A. C. Stuart, Langmuir **24** (2008) 6575.
21. O. Hollmann, C. Reichhart, and C. Czeslik, Z. Phys. Chem. **222** (2008) 205.
22. E. Bittrich, Rodenhausen KB, Eichhorn KJ, T. Hofmann, M. Schubert, M. Stamm, and P. Uhlmann, Biointerphases **5** (2010) 1.
23. N. D. Treat, N. Ayres, S. G. Boyes, and W. J. A. Brittain, Macromolecules **39** (2006) 26.
24. M. Ballauff, Prog. Polym. Sci. **32** (2007) 1135.

25. E. P. K. Currie, A. B. Sieval, M. Avena, H. Zuilhof, E. J. R. Sudholter, and M. A. C. Stuart, Langmuir **15** (1999) 7116.
26. E. P. K. Currie, W. Norde, and M. A. C. Stuart, Adv. Colloid Interf. Sci. **100** (2003) 205.
27. H. Kuroki, I. Tokarev, and S. Minko, Ann. Rev. Mater. Res. **42** (2012) 343.
28. A. Halperin and M. Kroger, Langmuir **25** (2009) 11621.
29. E. B. Zhulina and O. V. Borisov, Langmuir **27** (2011) 10615.
30. J. R. Howse, R. Steitz, M. Pannek, P. Simon, D. W. Schubert, and G. H. Findenegg, Phys. Chem. Chem. Phys. **3** (2001) 4044.
31. I. K. Voets, W. A. de Vos, B. Hofs, A. de Keizer, M. A. C. Stuart, R. Steitz, and D. Lott, J. Phys. Chem. B **112** (2008) 6937.
32. M. Gupta, T. Gutberlet, J. Stahn, P. Keller, and D. Clemens, Pramana-J. Phys. **63** (2004) 57.
33. M. Kreuzer, T. Kaltofen, R. Steitz, B. H. Zehnder, and R. Dahint, Rev. Sci. Instrum. (2011) 82.
34. N. Andrew, J. Phys. **251** (2010) 012094.
35. O. S. Heavens, *Optical Properties on Thin Solid Films* Dover Publications, Incorporated, Mineola, N.Y. (U.S.) (1955).
36. M. Tolan and W. Press, Z. Krist. **213** (1998) 319.
37. J. E. Mark, *Polymer Data Handbook* Oxford University Press, New York (1999).
38. V. F. Sears, Neutron News **3** (1992) 26.
39. D. C. Carter and J. X. Ho, Adv. Protein Chem. **45** (1994) 153.
40. R. R. Netz and M. Schick, Macromolecules **31** (1998) 5105.
41. E. A. DiMarzio and F. L. McCrackin, J. Chem. Phys. **43** (1965) 539.
42. A. Karim, S. K. Satija, J. F. Douglas, J. F. Ankner, and L. J. Fetters, Phys. Rev. Lett. **73** (1994) 3407.
43. P. Auroy, Y. Mir, and L. Auvray, Phys. Rev. Lett. **69** (1992) 93.
44. J. F. J. Dippy, S. R. C. Hughes, and A. Rozanski, J. Chem. Soc. (1959) 1441.
45. T. Miyajima, M. Mori, S. Ishiguro, K. H. Chung, and C. H. Moon, J. Colloid Interf. Sci. **184** (1996) 279.
46. A. Halperin, Langmuir **15** (1999) 2525.
47. M. L. Ferrer, R. Duchowicz, B. Carrasco, J. G. de la Torre, and A. U. Acuna, Biophys. J. **80** (2001) 2422.
48. F. L. G. Flecha and V. Levi, Biochem. Mol. Biol. Edu. **31** (2003) 319.
49. A. Halperin, G. Fragneto, A. Schollier, and M. Sferrazza, Langmuir **23** (2007) 10603.
50. Y. V. Lyatskaya, F. A. M. Leermakers, G. J. Fleer, E. B. Zhulina, and T. M. Birshtein, Macromolecules **28** (1995) 3562.
51. A. Baszkin and W. Norde, *Physical Chemistry of Biological Interfaces* CRC Press, New York, Basel (1999).
52. K. Nakanishi, T. Sakiyama, and K. Imamura, J. Biosci. Bioeng. **91** (2001) 233.